

The Sensitivity of the Redshift Distribution to Galaxy Demographics

Philipp Sudek^{1*}, Lucia F. de la Bella¹, Adam Amara¹, and William G. Hartley²

¹*Institute of Cosmology and Gravitation, University of Portsmouth, Portsmouth, PO1 3FX, UK*

²*Department of Astronomy, University of Geneva, ch. d'Ecogia 16, CH-1290 Versoix, Switzerland*

Accepted 2022 August 12. Received 2022 August 12; in original form 2022 January 11

ABSTRACT

Photometric redshifts are commonly used to measure the distribution of galaxies in large surveys. However, the demands of ongoing and future large-scale cosmology surveys place very stringent limits on the redshift performance that are difficult to meet. A new approach to meet this precision need is forward modelling, which is underpinned by realistic simulations. In the work presented here, we use simulations to study the sensitivity of redshift distributions to the underlying galaxy population demographics. We do this by varying the redshift evolving parameters of the Schechter function for two galaxy populations, star-forming and quenched galaxies. Each population is characterised by eight parameters. We find that the redshift distribution of shallow surveys, such as SDSS, is mainly sensitive to the parameters for quenched galaxies. However, for deeper surveys such as DES and HSC, the star-forming parameters have a stronger impact on the redshift distribution. Specifically, the slope of the characteristic magnitude, a_M , for star-forming galaxies has overall the strongest impact on the redshift distribution. Decreasing a_M by 148 per cent (its given uncertainty) shifts the mean redshift by ~ 45 per cent. We explore which combination of colour and magnitude measurements are most sensitive to a_M and we find that each colour-magnitude pair studied is similarly affected by a modification of a_M .

Key words: galaxies: distances and redshifts – galaxies: luminosity function – software: simulation

1 INTRODUCTION

The current standard model of cosmology, the Λ cold dark matter (Λ CDM) model, describes a universe consisting of dark energy, cold dark matter and baryonic matter evolving with time. At the present time, the energy density of the Universe is mainly determined by the dark energy and the dark matter components. However, these components are not fully understood yet and have to be better constrained (e.g. Clifton et al. 2012; Capela et al. 2013; Spergel 2015).

With different cosmological probes, we can shed some light on the dark parts of cosmology and constrain the parameters of dark energy and dark matter. Type Ia supernovae, the cosmic microwave background (CMB) and weak gravitational lensing (e.g. Albrecht et al. 2006; Nicola et al. 2017) are important probes. For example, constraining the equation-of-state parameter is an important objective of cosmic shear surveys. Most of these probes depend on the accurate prediction of the redshift distribution of galaxies,

$n(z)$. Using spectroscopy is the most precise way to determine the redshifts of galaxies. By identifying absorption and emission lines, one can calculate the redshift of the corresponding object. Although, these so-called ‘spectroscopic’ redshifts are not a suitable choice for current and upcoming experiments such as the Dark Energy Survey¹; the Hyper Suprime-Cam² of the Subaru Telescope; the Sloan Digital Sky Survey³; the Rubin Observatory Legacy Survey of Space and Time⁴ (LSST) and Euclid⁵. The big areas and depths observed by these surveys make performing the required spectroscopy extremely time-consuming and cost-intensive (Amara & Réfrégier 2007; Abdalla et al. 2008).

As an example, the Dark Energy Survey (DES, The Dark Energy Survey Collaboration 2005) is a ground-based telescope observing 5000 deg² of the Southern Sky in the vis-

¹ <https://www.darkenergysurvey.org>

² <https://hsc.mtk.nao.ac.jp/ssp/>

³ <https://www.sdss.org>

⁴ <https://www.lsst.org>

⁵ <https://sci.esa.int/web/euclid/>

* E-mail: philipp.sudek@port.ac.uk

ible spectrum. It uses the Dark Energy Camera (DECam, Honscheid & DePoy 2008; Flaugher et al. 2015) to observe more than 300 million galaxies. The DES standard band-passes are the DECam g , r , i , z and Y filters⁶ spanning a wavelength range from 400 to 1065 nm with a depth of $i = 23.44$ (in Data Release 1, Abbott et al. 2018).

Another example is the Hyper Suprime-Cam of the Subaru Telescope⁷ (HSC, Miyazaki et al. 2012). It covers 1400 deg² in the wide field, 27 deg² in the deep field and 3.5 deg² in the ultra-deep field. HSC consists of five broad-band filters and four narrow-band filters (Kawanomoto et al. 2018). The broad-band filters, g , r , i , z and y , cover a wavelength range of ~ 400 nm to ~ 1100 nm. The i -band limiting magnitude is 26.2 in the wide layer, 27.1 in the deep layer and 27.7 in the ultra-deep layer (Aihara et al. 2018).

The Sloan Digital Sky Survey (SDSS, York et al. 2000) has a lower depth. While taking data in the u , g , r , i and z filter bands⁸ the i -band limiting magnitude is 21.3 (Stoughton et al. 2002). The covered area is 14555 deg². Therefore, SDSS is measuring a much larger part of the sky compared to DES and HSC. The filters of SDSS cover a wavelength range of 300 nm to 1100 nm⁹.

For such big surveys, photometry is an alternative to spectroscopy. Photometric redshifts can be determined in two ways. First, one can fit the spectral energy distribution (SED) in different broad-band filters. The approach is to use different SED templates and fit them to the observed fluxes. Through this process, one gains information about the galaxies' redshifts (Bolzonella et al. 2000; Benitez 2000). Alternatively, photometric redshifts can be estimated by using machine learning methods (Carrasco Kind & Brunner 2013; Sadeh et al. 2016). This would require a sample of known redshifts to train the algorithm that determines the redshifts of the investigated sample. With template fitting and machine learning methods, we are able to get redshift estimates even for deep surveys. The problem is, the constraining power of cosmological probes that require redshift distributions is decreased by the lack of precision in the photometric redshifts (Bordoloi et al. 2010, 2012; Salvato et al. 2019).

To solve the problems of spectroscopic and photometric redshifts, Herbel et al. (2017) developed a method to simulate the redshift distribution directly. The authors used Approximate Bayesian Computation with a forward modelling approach to determine a full posterior of $n(z)$ without measuring the individual redshifts and which can be used in measurements. Thus, one does not rely on the technically challenging spectroscopic redshifts for big surveys. Furthermore, this approach delivers a more precise estimate of the redshift distribution than photometry.

In this paper, our main goal is to study the sensitivity of the redshift distribution of sets of galaxies to the underlying galaxy population properties. The motivation is to better understand which features of galaxy populations need to be

well understood to make the next generation of precision cosmological measurements.

To achieve our goal, we simulate galaxy catalogues solely with Herbel et al. (2017)'s forward modelling approach based on redshift-dependent Schechter luminosity functions, which describe the populations of different galaxy types. We analyse how changes of the Schechter luminosity function impact the redshift distribution for different survey types. Precisely, we identify the model parameters (Schechter parameters) that affect the simulations of the redshift distribution for the different survey types the most. Hence, this work demonstrates which parameters need better constraints to improve the precision of the simulated redshift distribution. This information will be important for the analysis of next generation precision measurements.

Furthermore, we investigate how the Schechter parameters affect the galaxy observables (apparent magnitude and colour distributions). As the magnitude and colour distributions are directly measurable quantities, this helps us to understand how the model parameters impact observations. In addition to this, this analysis identifies the observables that are most sensitive to the Schechter parameters and could help to constrain these parameters in the future.

In our analysis, we considered two different galaxy populations, a star-forming and a quenched model. Additionally, we chose the same parametric model as Herbel et al. (2017) to assign spectra to the galaxies. These spectra are used to calculate the apparent magnitudes of the galaxies. We simulated observed galaxy catalogues for DES-, SDSS- and HSC-like surveys. The catalogues contain the redshift values, absolute Johnson B -band magnitudes, intrinsic¹⁰ apparent magnitudes in different filter bands, observed¹¹ apparent magnitudes in different filter bands and the errors of the apparent magnitudes.

To perform the simulations, we used SkyPy (SkyPy Collaboration 2020; Amara et al. 2021). SkyPy is a publicly available python package for simulating the astrophysical sky and includes physical and empirical models for different observables. Therefore, SkyPy can be used to perform end-to-end simulations of these observables. We extended the code to account for observational errors and to obtain the observed magnitudes. A detailed description of this is summarised in section 3.

Furthermore, to account for signal-to-noise and saturation effects, we applied survey specific magnitude cuts in the i -band that remove too bright and too faint galaxies. We investigated the sensitivity of the redshift, colour and magnitude distributions to the different Schechter parameters by repeating the simulation after changing one parameter value by the range allowed by its uncertainty. The resulting catalogue was used as our test catalogue and compared to the fiducial catalogue¹².

This paper is structured as follows. In section 2, we summarise the mathematical models of our simulations. Section 3 presents our simulation set-up including the fiducial

⁶ <http://www.ctio.noao.edu/noao/node/13140>

⁷ <https://subarutelescope.org/en/>

⁸ Note that although we used the same notation for some of the DES, HSC and SDSS filter bands, we mean the filters specific to the surveys. For example, the g -band of DES, HSC and SDSS are different.

⁹ <https://www.sdss.org/instruments/camera/>

¹⁰ Observational error not considered

¹¹ The word "observed" indicates that the magnitudes include an observational error. We describe the simulation of the error in section 3.3.1.

¹² Catalogue that was simulated with the default set of Schechter luminosity function parameters. See sections 3 and 4.

Schechter parameters, a detailed description of our error model and how we perform the magnitude cuts. In section 4, we describe the methodology of our simulations and the comparison of fiducial and test catalogue. Our results are presented in section 5 and section 6 includes our conclusions. Throughout this work, we use a standard Λ CDM cosmology with $h = 0.7$, $\Omega_m = 0.3$ and $\Omega_\Lambda = 0.7$.

2 FORWARD MODELLING GALAXY CATALOGUES

In this section, we describe our model for simulating galaxy catalogues including redshifts, magnitudes and colours. Our simulations follow a forward modelling approach to draw galaxies from the Schechter luminosity function, as described by Herbel et al. (2017). We assign the redshifts and absolute B -band magnitudes that follow the Schechter luminosity function to our objects. With these quantities, we calculate the apparent magnitudes in different filter bands by simulating the spectra that are based on template coefficients. A deeper investigation and motivation of this model will be the scope for future work.

2.1 Luminosity Function and Galaxy Numbers

Generating intrinsic galaxy catalogues requires a model of the expected galaxy number in a certain volume of the sky. The luminosity function Φ describes the number of galaxies N per comoving volume V and absolute magnitude M as a function of redshift z ,

$$\Phi(z, M) = \frac{dN}{dV dM}. \quad (1)$$

Different observations (Loveday et al. 2012; López-Sanjuan et al. 2017) have supported the work from Schechter (1976) that described the functional form of the luminosity function. The Schechter luminosity function is given as

$$\Phi(z, M) = 0.4 \ln(10) \Phi_*(z) 10^{0.4(M_*(z) - M)(\alpha(z) + 1)} \cdot \exp\left(-10^{0.4(M_*(z) - M)}\right), \quad (2)$$

where the faint-end-slope α , the characteristic magnitude M_* and the amplitude Φ_* are free-fitting parameters. These parameters depend on the type of the galaxy population and on the redshift.

The evolution of the luminosity function with redshift can be empirically motivated (Herbel et al. 2017). Keeping α constant for each galaxy population, the characteristic magnitude and the amplitude are parametrised as

$$M_*(z) = a_M z + b_M, \quad (3)$$

$$\Phi_*(z) = b_\phi \exp(a_\phi z). \quad (4)$$

Combined each population is described by five parameters. However, we assume that each type evolves according to the same functional form. In this paper, we refer to the parameters a_M , b_M , a_ϕ and b_ϕ as the ‘‘Schechter parameters’’ as these are the model parameters we investigated.

Considering the volume element as a light cone, we can write the comoving element in terms of the solid angle Ω and redshift z as

$$dV = \frac{d_H d_M^2}{E(z)} d\Omega dz, \quad (5)$$

where d_H is the Hubble distance, d_M is the transverse comoving distance and $E(z) = (\Omega_m(1+z)^3 + \Omega_k(1+z)^2 + \Omega_\Lambda)^{0.5}$. Plugging this into equation 1, we get the number of galaxies per absolute magnitude, redshift and solid angle

$$\phi(z, M) = \frac{dN}{dM d\Omega dz} = \frac{d_H d_M^2}{E(z)} \Phi(z, M). \quad (6)$$

This function is the number density which can be used to draw samples of galaxies. These samples contain redshift values and absolute magnitudes that follow the distribution ϕ . Additionally, by integrating equation 6, one obtains the number of galaxies that would be observed in a light cone, spanned by solid angle Ω with redshifts between z_1 and z_2 and magnitudes between M_1 and M_2 ,

$$N(z_1, z_2, M_1, M_2, \Omega) = \Omega \int_{M_1}^{M_2} \int_{z_1}^{z_2} \phi(z, M) dz dM. \quad (7)$$

2.2 Galaxy Colours

The colour of a galaxy is defined as the difference in its magnitudes in two different filter bands. Given the spectrum $f(\lambda)$ of a galaxy, calculating the magnitude in a particular band is straightforward.

First, the absolute magnitude in this band has to be calculated. In the AB magnitude system, this is given as (Blanton et al. 2003)

$$M_i = -2.41 - 2.5 \log_{10} \left[\frac{\int_0^\infty d\lambda_o \lambda f(\lambda) R(\lambda_o)}{\int_0^\infty d\lambda_o \lambda^{-1} R(\lambda_o)} \right], \quad (8)$$

where $R(\lambda)$ is the filter response giving the fraction of photons that are included in the signal. The subscript ‘o’ indicates the observed frame and the observed and emitted wavelengths are related through the redshift relation $\lambda_o = (1+z)\lambda$. The units of the spectrum $f(\lambda)$ are $\text{erg s}^{-1} \text{cm}^{-2} \text{\AA}^{-1}$ in this equation. To transform this into an apparent magnitude, we employ the distance modulus, $DM(z) = 5 \log_{10}(d_L(z)/10 \text{ pc})$, where d_L is the luminosity distance. Thus, the apparent magnitude in band i is given by

$$m_i = M_j + DM(z) + K_{ji}(z), \quad (9)$$

with $K_{ji}(z)$ accounting for the K correction (Hogg et al. 2002; Blanton & Roweis 2007), which is relating the emitted rest-frame magnitude in broad photometric bandpass j to the observed apparent magnitude in band i .

2.3 Galaxy Spectra

Simulating the magnitudes of the galaxies requires the galaxies’ spectra. To model the spectrum, we again follow the approach of Herbel et al. (2017), which is based on the work by Blanton & Roweis (2007). The flux density as it would be seen if the galaxy is at a distance of 10 pc is given as a linear combination of five template spectra $t_i(\lambda)$,

$$f(\lambda) = \sum_i c_i t_i(\lambda), \quad (10)$$

where the units of $f(\lambda)$ are $\text{erg s}^{-1} \text{cm}^{-2} \text{\AA}^{-1}$ per solar mass. Herbel et al. (2017) showed that after re-weighting the coefficients c_i by a weight w_i , the coefficients follow a Dirichlet distribution of order five so that $\sum_i \tilde{c}_i = 1$ with $\tilde{c}_i = c_i/w_i$.

A Dirichlet distribution (Kotz et al. 2019) of order $K \geq 2$ is defined as

$$\text{Dir}(x_1, \dots, x_K; \alpha_1, \dots, \alpha_K) = \frac{1}{B(\boldsymbol{\alpha})} \prod_{i=1}^K x_i^{\alpha_i - 1}, \quad (11)$$

where $\boldsymbol{\alpha} = (\alpha_1, \dots, \alpha_K)$ with $\alpha_i > 0$ are parameters characterising the Dirichlet distribution and $B(\boldsymbol{\alpha})$ is the multivariate beta function.

Therefore a Dirichlet distribution of order five is characterised by five parameters α_i . These parameters are redshift dependent in general. Once again according to Herbel et al. (2017), we assume that the evolution of the parameters is described as

$$\alpha_i(z) = (\alpha_{i,0})^{1-z/z_1} \cdot (\alpha_{i,1})^{z/z_1}. \quad (12)$$

The two parameters $\alpha_{i,0}$ and $\alpha_{i,1}$ describe the galaxy population at redshift $z = 0$ and $z = z_1 > 0$, respectively. They are also different for each galaxy type.

Note that the K-correct templates $t_i(\lambda)$ are intended to fit broad-band photometry, which is suitable for our case. In this work, we decided to build on the studies presented in Herbel et al. (2017), Fagioli et al. (2018, 2020) and Tortorelli et al. (2018, 2020, 2021), which show that the K-correct templates can be used in our analysis, especially at low redshifts. We are also revisiting the quality of the templates for higher redshifts in a new study (Hartley et al. in prep), which will show that this model predicts colour and apparent magnitude distributions even for samples with higher redshifts.

3 SIMULATION SETUP

In this section, we describe the setup of our simulations. We summarise how the fiducial catalogues of each survey were generated based on the model described in section 2. That includes the Schechter parameters, the Dirichlet parameters for generating the spectra, the simulated sky area and filter bands of each survey type.

Furthermore, we describe how the intrinsic catalogues are transformed into observed galaxy catalogues for each survey. Additionally, we explain our choice of magnitude cuts to mock real observations.

3.1 Schechter Parameters

In our work, we used the parameters from Tortorelli et al. (2021) following a model consisting of star-forming and quenched galaxies. Table 1 summarises the values of the Schechter parameters together with their errors.

As aforementioned, each galaxy population can be simulated by drawing from the same distribution with different parameters. The redshift dependency of our model is given by the faint-end slope α , the characteristic magnitude M_* and the amplitude of the Schechter function Φ_* . In equations 3 and 4, we parametrise M_* as a linear function and Φ_* as an exponential function of redshift z . Therefore, our model is described by five parameters, α , a_M , b_M , a_ϕ and b_ϕ .

In our investigation, α was considered redshift independent such that only four parameters characterised the evolution with redshift. We focused on this set of parameters and investigated the sensitivity of the redshift distribution to a

Table 1. Schechter Parameters for our simulations. Values and errors are taken from Tortorelli et al. (2021). The positive and negative errors correspond to the 84th percentile and 50th percentile values, respectively.

Parameter	Star-Forming	Quenched
α	-1.3	-0.5
a_M	$-0.439^{+0.535}_{-0.652}$	$-0.697^{+0.698}_{-0.729}$
b_M	$-20.623^{+0.417}_{-0.425}$	$-20.372^{+0.513}_{-0.466}$
a_ϕ	$-0.088^{+0.297}_{-0.277}$	$-0.836^{+0.812}_{-0.733}$
b_ϕ	$0.004245^{+0.001337}_{-0.001452}$	$0.005169^{+0.003112}_{-0.003515}$

Table 2. Dirichlet parameters α_i and weights w_i for our simulations. The Dirichlet parameters are taken from Tortorelli et al. (2018) and the weights are from Herbel et al. (2017).

Parameter	Star-Forming	Quenched
α_1	1.9946549	1.62158197
α_2	1.99469164	1.62137391
α_3	1.99461187	1.62175061
α_4	1.9946589	1.62159144
α_5	1.99463069	1.62165971
w_1	$3.47 \cdot 10^9$	$3.84 \cdot 10^9$
w_2	$3.31 \cdot 10^6$	$1.57 \cdot 10^6$
w_3	$2.13 \cdot 10^9$	$3.91 \cdot 10^8$
w_4	$1.64 \cdot 10^{10}$	$4.66 \cdot 10^{10}$
w_5	$1.01 \cdot 10^9$	$3.03 \cdot 10^7$

change in these parameters for the different surveys. Since the parameters have different values according to the galaxy type, we had one set of four parameters for the star-forming galaxies and another set of four parameters for the quenched galaxies.

3.2 Dirichlet Parameters

Table 2 summarises the Dirichlet parameters from Tortorelli et al. (2018) and the weights from Herbel et al. (2017).

As we explained in section 2, we simulated the spectra based on template coefficients that are drawn from a Dirichlet distribution. We considered a model independent of redshift such that $\alpha_i(z)$ from equation 12 is a constant (just denoted as α_i from here on).

To account for the different galaxy types, we also introduced weights for each coefficient (more details in Herbel et al. (2017)). Through the distinction between star-forming and quenched galaxies, we had a total of ten parameters and their corresponding weights, respectively.

3.3 Surveys and Observed Catalogues

We identified the Schechter parameters that have the biggest impact on the simulated redshift distribution of different surveys. Within the context of the Herbel et al. (2017) forward modelling approach, having more precise parameter values

Table 3. Summary of the investigated surveys including the simulated filter bands, sky area and the resulting number of galaxies of each fiducial catalogue.

Survey	Filter Bands	Sky Area	Number of Galaxies
DES	g, r, i, z	10 deg ²	~58500
SDSS	u, g, r, i, z	135 deg ²	~59300
HSC	g, r, i, z, y	1.75 deg ²	~58400

directly translates into better cosmological constraints that are based on the redshift distribution.

Moreover, we analysed the effect of the Schechter parameters on three survey types, based on their depths and fields of view. We investigated a DES-like survey, a deeper but narrower HSC deep-field-like survey and a shallower but wider SDSS-like survey. These surveys have different sets of filter bands, which we needed to reflect in the simulations.

With the SkyPy python package, we applied these filters directly. We chose to simulate the DES-like survey with the DECam g, r, i and z filters. In the case of HSC, we used the g, r, i, z and y filters. To simulate the SDSS-like catalogue, we used the SDSS u, g, r, i and z filters.

Since the leading order effect of precision measurements is usually the number of galaxies, we simulated different fields of view for each survey. Thus, we had approximately the same number of galaxies in each fiducial catalogue and could explore the trends beyond pure number counts. We chose a simulated area of 10 deg² for DES, 1.5 deg² in the case of HSC and 135 deg² for SDSS. That resulted in ~58500 galaxies in the DES-like fiducial observed catalogue, ~59300 in the SDSS-like catalogue and ~58400 galaxies in the HSC-like catalogue. A summary of the filter bands, sky area and the resulting number of galaxies of our fiducial catalogues is given in table 3.

To make the intrinsic catalogues of the surveys observed catalogues, we performed two additional steps in our simulations:

- (i) Adding survey specific errors to the simulated intrinsic magnitudes
- (ii) Applying survey specific magnitude cuts

3.3.1 Modelling Magnitude Uncertainties

In sections 3.1 and 3.2, we described the setup to simulate intrinsic catalogues. However, making realistic simulations of galaxy catalogues implies modelling the magnitude uncertainties appropriately. These uncertainties must be specific to the survey. We used Rykoff et al. (2015)'s model to simulate the uncertainty, σ_m , of the apparent magnitudes in each filter band for every survey,

$$\sigma_m(F; F_{\text{noise}}, t_{\text{eff}}) = \frac{2.5}{\ln 10} \left[\frac{1}{F t_{\text{eff}}} \left(1 + \frac{F_{\text{noise}}}{F} \right) \right]^{1/2}, \quad (13)$$

where

$$F = 10^{-0.4(m - m_{\text{ZP}})} \quad (14)$$

is the galaxy's flux,

$$F_{\text{noise}} = \frac{F_{\text{lim}}^2 t_{\text{eff}}}{10^2} - F_{\text{lim}} \quad (15)$$

is the effective noise flux and t_{eff} is the effective exposure time¹³. Furthermore, m is the galaxy's magnitude, m_{ZP} is the zero-point magnitude of the filter band and F_{lim} is the 10σ limiting flux.

Equations 13, 14 and 15 then define the uncertainty of the magnitude, $\sigma_m(m; m_{\text{lim}}, t_{\text{eff}})$, depending on magnitude m , limiting magnitude m_{lim} (magnitude associated with F_{lim}) and effective exposure time t_{eff} . We also used the same model as Rykoff et al. (2015) for the effective exposure time,

$$\ln t_{\text{eff}} = a + b(m_{\text{lim}} - 21), \quad (16)$$

where a and b are free parameters.

We fitted $\sigma_m(m)$ (i.e. fitting a and b) to measured data. In this way, we got the magnitude uncertainties specific to the survey. For the zero-point magnitudes m_{ZP} , we used a value of 30 for each filter band and every survey. That is justified because this model is only an approximation and has initially been developed for SDSS data only. The model is empirically motivated and does not include any deeper analysis of signal-to-noise effects that exist during observations.

Figures 1, 2 and 3 show the fitted magnitude uncertainties in each filter band and compare them to the data for every survey type, respectively. We see that the fits agree very well with the data in the regions of high galaxy density for each survey type. In the case of DES- and HSC-like surveys, in figures 1 and 3, we observe that there are minor deviations of model and data in the region of small magnitudes and errors. Since the error values are very small compared to the magnitude values in this region, we do not expect these deviations to impact our simulations and analysis majorly. In the case of SDSS-like surveys in figure 2, the fits are less good compared to DES- and HSC-like surveys. However, we used the results presented in Rykoff et al. (2015) and did not perform our own fits. The largest deviations of fit and data are again in the region of small error such that they do not impact our analysis majorly. Further, please note that our goal was not to simulate the magnitude-error correlation perfectly, but to have a model that describes the relationship sufficiently. In the plots, we can see that we achieved this goal although the given limiting magnitudes of SDSS and HSC do not correspond to 10σ magnitude limits.

Tables 4, 5 and 6 summarise the fit results and the used magnitude limits. As mentioned, we used the fit results from Rykoff et al. (2015) in the case of the SDSS-like survey. For the DES-like survey, we performed the fit to the Y1 results and used the corresponding limiting magnitudes as described by Drlica-Wagner et al. (2018). For SDSS, we compared the fit to DR16 data (Ahumada et al. 2020) and used the limiting magnitudes described in Stoughton et al. (2002). Regarding HSC, we fitted DR2 data and used the magnitude limits of the deep survey described in Aihara et al. (2019).

The modelled uncertainties were used to assign an error to the intrinsic magnitudes. We drew Gaussian random variables with mean zero and the standard deviations being the

¹³ Note that we absorbed the normalisation constant k , which is mentioned in Rykoff et al. (2015), in the definition of t_{eff} .

Table 4. Fit results of the magnitude uncertainty and used magnitudes limits of each filter band for a **DES-like survey**. The parameters a and b describe the effective exposure time in equation 16. The fit was performed to DES Y1 (Drlica-Wagner et al. 2018) data and the corresponding magnitudes limits were taken from Drlica-Wagner et al. (2018).

Filter Band	a	b	m_{lim}
g	1.541275	-1.000737	23.4
r	-0.743079	-0.116539	23.2
i	0.846085	-1.660630	22.5
z	-0.044378	-2.774705	21.8

Table 5. Fit results of the magnitude uncertainty and used magnitudes limits of each filter band for an **SDSS-like survey**. The parameters a and b describe the effective exposure time in equation 16. The fit results were taken from Rykoff et al. (2015) and the corresponding magnitudes limits were taken from Stoughton et al. (2002).

Filter Band	a	b	m_{lim}
u	3.41	1.15	22
g	4.27	0.85	22.2
r	4.53	0.91	22.2
i	4.56	1.00	21.3
z	4.39	1.34	20.5

Table 6. Fit results of the magnitude uncertainty and used magnitudes limits of each filter band for an **HSC-like survey**. The parameters a and b describe the effective exposure time in equation 16. The fit was performed to HSC DR2 (Aihara et al. 2019) data and the corresponding magnitudes limits were taken from Aihara et al. (2019).

Filter Band	a	b	m_{lim}
g	135.095407	20.425863	27.8
r	-2.270331	0.924841	27.4
i	-0.272460	0.563884	27.1
z	-0.707218	0.618222	26.6
y	61.117607	13.634286	25.6

modelled uncertainties. We added the random values to the intrinsic magnitudes and generated the observed catalogue.

3.3.2 Magnitude Cuts

To generate mock observed catalogues, we needed to account for further observational effects. Besides environmental factors like weather, which we did not include, signal-to-noise effects had to be addressed in our simulations. Taking observations, only measurements that exceed a certain signal-to-noise threshold are kept, which guarantees the quality of the data. Fainter sources are more affected than brighter objects because the noise does not linearly scale with the brightness. The signal-to-noise ratio defines how deep a sur-

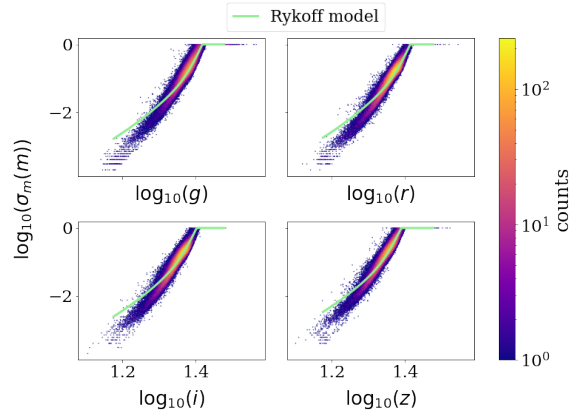


Figure 1. Magnitude uncertainties of a **DES-like survey**. The binned data points

show the DES Y1 measurements (Drlica-Wagner et al. 2018) of the apparent magnitudes and its corresponding uncertainties, $\sigma_m(m)$, in the g , r , i and z filter bands. The green lines show the respective fits to the Rykoff et al. (2015) error model. We see that model and data generally match.

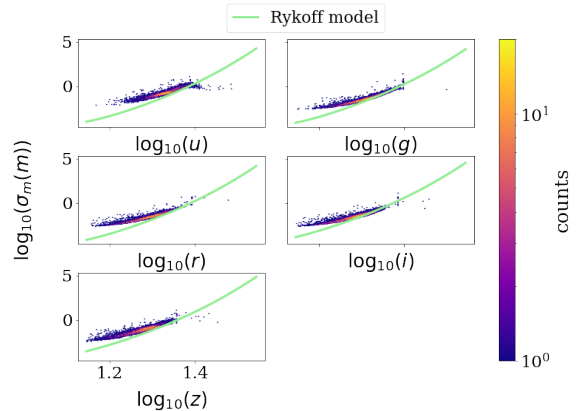


Figure 2. Magnitude uncertainties of an **SDSS-like survey**. The binned data points show the SDSS DR16 measurements (Ahumada et al. 2020) of the apparent magnitudes and its corresponding uncertainties, $\sigma_m(m)$, in the u , g , r , i and z filter bands. The green lines show the respective fits to the Rykoff et al. (2015) error model. We see that model and data generally match for most of the data points.

vey is and sets a lower limit on the brightness of an object to be observed.

However, signal-to-noise selection is a complex process and mocking it is not straightforward. Simulating realistic signal-to-noise for galaxies needs to account for large sets of galaxy properties (such as luminosity, size, profile and ellipticity) and how these correlate with the point-spread-function properties (size and shape) at the positions of galaxies (Bergé et al. 2013; Herbel et al. 2017). This means that we would need to implement realistic image simulations to fully account for signal-to-noise selection effects, which exceeds the purpose of our paper. Therefore, we have fo-

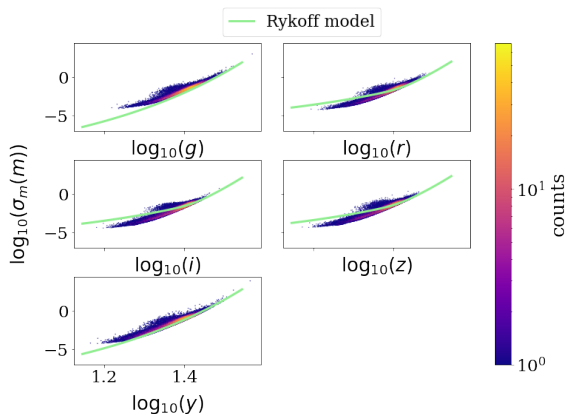


Figure 3. Magnitude uncertainties of a **HSC-like survey**. The binned data points show the HSC DR2 measurements (Aihara et al. 2019) of the apparent magnitudes and its corresponding uncertainties, $\sigma_m(m)$, in the g , r , i , z and y filter bands. The green lines show the respective fits to the Rykoff et al. (2015) error model. We see that model and data generally match.

Table 7. The upper and lower magnitude limits that were used in our analysis. Only objects with i -band magnitudes between i_{lower} and i_{upper} were kept in the catalogues.

Survey	i_{upper}	i_{lower}
DES	24	18
SDSS	21	18
HSC	27	18

cused on a fixed magnitude cut where the sample should be complete.

In our work, we chose a cut in the i -band. That means all objects whose i -band magnitude is fainter than a certain cut-off point i_{upper} were removed. As the investigated surveys have varying depths, the respective upper-cut magnitudes were different. In the case of a DES-like survey, we chose $i_{\text{upper,DES}} = 24$ and for an HSC-like survey, we used $i_{\text{upper,HSC}} = 27$. In the case of SDSS, $i_{\text{upper,SDSS}}$ were 21.

The saturation of pixels is another crucial effect that occurs during observations. If a source is too bright, too many photons are detected by the CCD and pixels start to saturate. To account for this, we introduced a magnitude cut for bright objects. Again, we used a cut in the i -band. However, the cut was the same for each survey. We removed all objects with i -band magnitudes brighter than $i_{\text{lower}} = 18$. Table 7 summarises all cuts that were used in our work.

4 METHOD

In this section, we describe the method that we used to investigate the sensitivity of the redshift distribution to the Schechter parameters and the impact of those parameters to the observables.

First, we simulated the intrinsic fiducial galaxy catalogues for all surveys. To do this, we used the SkyPy Python package, which enables us to perform the simulations ac-

ording to the model described in section 2. The intrinsic catalogues contained redshift values, absolute Johnson B-band magnitudes and apparent magnitudes in different filter bands specific to the survey. We summarised the fiducial values of the parameters in sections 3.1 and 3.2.

Afterwards, the intrinsic catalogues were transformed into observed catalogues. We added an observational error to the apparent magnitudes and performed magnitude cuts to remove too faint and too bright objects. We refer to section 3.3 for further details.

To analyse the sensitivity of the surveys to the different Schechter parameters, we changed the value of one of the parameters by adding and subtracting its error and repeated the whole simulation process as described in the previous paragraphs. The positive and negative errors correspond to the 84th and 50th percentile values, respectively. Note, the sensitivity is relative to the ability of modern datasets to constrain the parameters (see table 2). Modifying the parameter changed the luminosity function and the simulation resulted in a galaxy catalogue with different redshift, magnitude and colour distributions. We call this catalogue the “test” catalogue. Remember that the sample is defined by the Schechter parameters and the Dirichlet coefficients. We concentrated on the effect of the Schechter parameters on the redshift distribution. The correlation between the parameters and coefficients, if there is one, has not been measured in the literature and determining this correlation is beyond the scope of our paper.

Comparing the redshift distributions of fiducial and test catalogue allowed us to identify the sensitivity of the survey’s redshift distribution to the modified parameter. By comparing the colour and magnitude distributions of fiducial and test catalogue, we diagnosed different observables (magnitude or colour distribution) that are sensitive to a change in the parameter value and, thus, could be used to constrain the parameters.

In this context, “sensitive to a Schechter parameter” means that the redshift distribution of the galaxy catalogue changes after modifying the parameter. Furthermore, a greater change indicates a higher sensitivity of this survey to the parameter. Accordingly, an observable has better constraining ability if it is more affected by the parameter change.

4.1 Investigating Redshift Sensitivity

Since the mean of the redshift distribution is the leading order term in weak lensing analyses (Tessore & Harrison 2020), we concentrated on the change of the mean redshift. Comparing the mean redshift of the fiducial and the test redshift distributions is beneficial in several ways. First, one can investigate the absolute change that informs about the required precision of the parameter. Second, the relative change reveals the parameter that has the strongest impact on the redshift distribution.

We define the relative change as

$$\delta z_{\text{mean}} = \frac{|\Delta z_{\text{mean}}|}{\bar{z}_{\text{fid}}}, \quad (17)$$

where $\Delta z_{\text{mean}} = \bar{z}_{\text{test}} - \bar{z}_{\text{fid}}$ is the absolute change of the mean redshift, \bar{z}_{test} is the mean redshift of the test catalogue and \bar{z}_{fid} is the mean redshift of the fiducial catalogue.

As the simulations are affected by statistical fluctuations, we made sure that the change of the mean redshift did not arise from statistical effects. To account for this, we generated 100 realisations of the fiducial and test catalogues. We then compared the mean redshifts by looking at the mean of δz_{mean} and Δz_{mean} over the 100 simulations. Hence, $\overline{\delta z_{\text{mean}}}$ and $\overline{\Delta z_{\text{mean}}}$ were more appropriate to quantify the change in the redshift distribution.

4.2 Important Observables

After identifying the parameters with the strongest impact on the redshift distribution, we focused on how the Schechter parameters affect the observables. Thus, we could find the observables that are most sensitive to the parameters and that could help constraining these parameters.

In our analysis, we compared the magnitude distributions and colour distributions of fiducial and test catalogues by using the Anderson-Darling (AD) test (Scholz & Stephens 1987; Feigelson & Babu 2012). For the test, we used the assumption that the two tested samples are drawn from the same distribution as the null hypothesis. The AD test is a statistical test measuring the sum of the squared differences of the distributions, d_{AD} . The sensitivity of the corresponding observable to the parameter increases with growing value of d_{AD} . The relating p-value describes the probability to obtain a test statistic d_{AD} at least as extreme as measured under the assumption that the null hypothesis is true.

As described in section 4.1, we ran 100 simulations to account for numerical noise. We calculated the 95-th percentiles of the 100 d-values, $d_{\text{AD},95}$, and p-values, $p_{\text{AD},95}$, for each observable. These values then indicated the change of the observable after changing the Schechter parameter. Furthermore, we looked for large values of $d_{\text{AD},95}$ and small values of $p_{\text{AD},95}$.

We repeated the whole process of simulating the test catalogues and comparing them to the fiducial catalogues for all eight Schechter parameters and all surveys. We performed the analysis after changing each parameter value by its given positive and negative error. That enabled us to identify which survey is sensitive to which parameters. In addition to this, we could determine which observables and which surveys show higher sensitivity to the specific parameters and can, therefore, be more useful in constraining the parameters.

5 RESULTS

This section describes the results of our analysis. We start with identifying the parameters that have the strongest effect on the redshift distribution of each survey in section 5.1. We finalise with the discussion about the impact of the Schechter parameters on the different observables in section 5.2.

5.1 Redshift Sensitivity

As described in section 4, we compared the redshift distributions of fiducial and test catalogue using sets of 100 simulations. The mean of the relative change, $\overline{\delta z_{\text{mean}}}$, and

the mean of the absolute change, $\overline{\Delta z_{\text{mean}}}$, of the mean redshift indicated the parameters with the highest impact on each survey. Tables 8, 9 and 10 summarise our results of the relative and absolute mean redshift change. They show the impact on the redshift distribution after updating each parameter in positive and negative directions.

Table 8 summarises the sensitivity of DES-like surveys. We found that a DES-like survey is most sensitive to $a_{\text{M,SF}}$. Decreasing $a_{\text{M,SF}}$ increases the mean redshift by ~ 45 per cent. This relative change corresponds to an absolute change of 0.304. The rest of the parameters have less impact on the mean redshift. However, $a_{\text{M,Q}}$, $a_{\phi,\text{Q}}$ and $b_{\text{M,SF}}$ can also have a significant effect on the redshift distribution. Updating these parameters causes relative changes of the mean redshift up to 13.5 per cent, which corresponds to an absolute change of 0.091.

Table 9 shows the results for an HSC-like survey. Again, $a_{\text{M,SF}}$ has the strongest impact on the redshift distribution. The mean redshift of an HSC-like survey changes by ~ 23 per cent after decreasing $a_{\text{M,SF}}$ by its negative error. Therefore, the uncertainty of $a_{\text{M,SF}}$ shifts the simulated mean redshift by up to ~ 0.26 . Furthermore, we found that the parameters $a_{\phi,\text{SF}}$ and $a_{\phi,\text{Q}}$ also have strong impact on the mean redshift. Increasing these parameters causes relative changes of ~ 12.4 per cent and ~ 8.7 per cent, which corresponds to absolute changes of about 0.14 and 0.10, respectively.

Finally, we focused on the redshift sensitivity of SDSS-like surveys. Table 10 presents the impact of the Schechter parameters on an SDSS-like redshift distribution. The parameter $a_{\text{M,Q}}$ has the strongest effect on the redshift distribution. The mean redshift changes by 10.5 per cent after decreasing $a_{\text{M,Q}}$. The corresponding absolute change of 0.036 illustrates that SDSS-like surveys are not strongly affected by the parameter uncertainties.

Figures A1, A2 and A3 in appendix A illustrate the differences in the fiducial and test redshift distributions for all survey types. The plots show the redshift distributions of which the summary statistics are given in tables 8, 9 and 10. Larger values of $\overline{\delta z_{\text{mean}}}$ correspond to visually larger differences in the distributions.

5.1.1 Survey Comparison

Figure 4 compares the fiducial and test redshift distributions for all survey types after modifying different parameters. Each plot shows the fiducial redshift distribution in black, the test redshift distribution after decreasing the corresponding parameter by 1σ in blue and the test redshift distribution after increasing the parameter by 1σ in red. The columns correspond to the different surveys, the first column shows the results for an SDSS-like survey, the second for a DES-like and the third for an HSC-like survey. Moreover, we compare the effect of three different parameters in the individual rows. The first row shows the impact of $a_{\text{M,SF}}$, the second of $a_{\phi,\text{Q}}$ and the third of $b_{\text{M,SF}}$. In addition, we indicate the number of galaxies per square arcminute in the legend of each plot.

The first row highlights that $a_{\text{M,SF}}$ has a higher impact on DES- and HSC-like surveys than on SDSS-like surveys. Decreasing $a_{\text{M,SF}}$ increases the mean redshift. Increasing $a_{\text{M,SF}}$ decreases the mean redshift. This effect also correlates with the galaxy number density. The second row shows

Table 8. Relative change, $\overline{\delta z_{\text{mean}}}$, and absolute change, $\overline{\Delta z_{\text{mean}}}$, of the mean redshift for a **DES-like survey**. The values correspond to the mean of 100 realisations. They indicate the change in the redshift distribution after increasing (Positive) and decreasing (Negative) the corresponding parameter by its given errors. Higher values of $\overline{\delta z_{\text{mean}}}$ indicate stronger sensitivity to the corresponding parameter. $\overline{\Delta z_{\text{mean}}}$ is a measure for the required precision of the mean redshift.

Parameter	Positive		Negative	
	$\overline{\delta z_{\text{mean}}}$ in %	$\overline{\Delta z_{\text{mean}}}$	$\overline{\delta z_{\text{mean}}}$ in %	$\overline{\Delta z_{\text{mean}}}$
$a_{\text{M,SF}}$	10.5	-0.071	44.9	0.304
$a_{\text{M,Q}}$	3.8	-0.026	13.5	0.091
$a_{\phi,\text{SF}}$	4.9	0.033	3.6	-0.024
$a_{\phi,\text{Q}}$	8.7	0.059	2.8	-0.019
$b_{\text{M,SF}}$	5.5	-0.037	7.7	0.053
$b_{\text{M,Q}}$	2.7	-0.018	3.5	0.024
$b_{\phi,\text{SF}}$	0.5	-0.004	1.0	0.007
$b_{\phi,\text{Q}}$	1.1	0.008	1.7	-0.012

Table 9. Relative change, $\overline{\delta z_{\text{mean}}}$, and absolute change, $\overline{\Delta z_{\text{mean}}}$, of the mean redshift for an **HSC-like survey**. The values correspond to the mean of 100 realisations. They indicate the change in the redshift distribution after increasing (Positive) and decreasing (Negative) the corresponding parameter by its given errors. Higher values of $\overline{\delta z_{\text{mean}}}$ indicate stronger sensitivity to the corresponding parameter. $\overline{\Delta z_{\text{mean}}}$ is a measure for the required precision of the mean redshift.

Parameter	Positive		Negative	
	$\overline{\delta z_{\text{mean}}}$ in %	$\overline{\Delta z_{\text{mean}}}$	$\overline{\delta z_{\text{mean}}}$ in %	$\overline{\Delta z_{\text{mean}}}$
$a_{\text{M,SF}}$	17.63	-0.2053	22.69	0.2643
$a_{\text{M,Q}}$	1.50	-0.0175	1.74	0.0203
$a_{\phi,\text{SF}}$	12.37	0.1441	9.29	-0.1082
$a_{\phi,\text{Q}}$	8.68	0.1011	1.18	-0.0138
$b_{\text{M,SF}}$	4.19	-0.0488	3.84	0.0447
$b_{\text{M,Q}}$	0.55	-0.0064	0.51	0.0059
$b_{\phi,\text{SF}}$	0.05	-0.0006	0.06	0.0007
$b_{\phi,\text{Q}}$	0.06	0.0007	0.13	-0.0015

Table 10. Relative change, $\overline{\delta z_{\text{mean}}}$, and absolute change, $\overline{\Delta z_{\text{mean}}}$, of the mean redshift for an **SDSS-like survey**. The values correspond to the mean of 100 realisations. They indicate the change in the redshift distribution after increasing (Positive) and decreasing (Negative) the corresponding parameter by its given errors. Higher values of $\overline{\delta z_{\text{mean}}}$ indicate stronger sensitivity to the corresponding parameter. $\overline{\Delta z_{\text{mean}}}$ is a measure for the required precision of the mean redshift.

Parameter	Positive		Negative	
	$\overline{\delta z_{\text{mean}}}$ in %	$\overline{\Delta z_{\text{mean}}}$	$\overline{\delta z_{\text{mean}}}$ in %	$\overline{\Delta z_{\text{mean}}}$
$a_{\text{M,SF}}$	3.8	-0.013	9.1	0.031
$a_{\text{M,Q}}$	5.8	-0.020	10.5	0.036
$a_{\phi,\text{SF}}$	0.9	0.003	0.7	-0.002
$a_{\phi,\text{Q}}$	4.8	0.016	3.3	-0.011
$b_{\text{M,SF}}$	2.7	-0.009	5.9	0.020
$b_{\text{M,Q}}$	7.1	-0.024	9.0	0.031
$b_{\phi,\text{SF}}$	1.5	-0.005	2.4	0.008
$b_{\phi,\text{Q}}$	2.7	0.009	5.4	-0.019

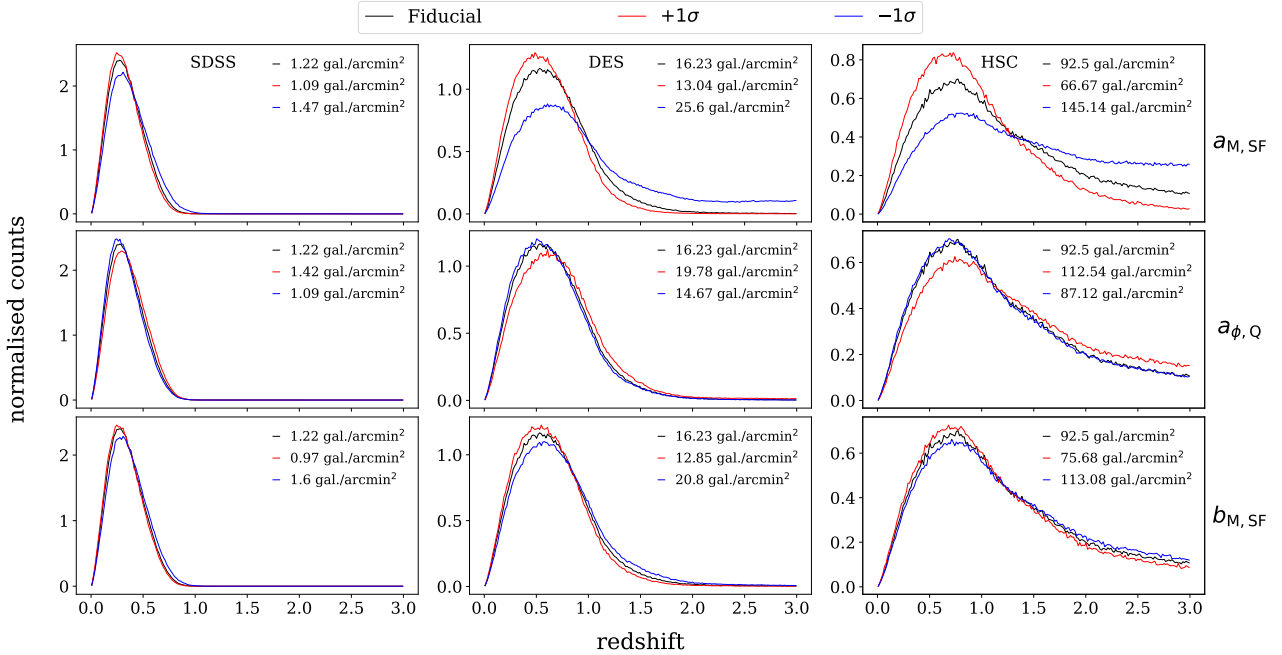


Figure 4. Comparison of the normalised simulated fiducial (black) and test redshift distributions after increasing (red) and decreasing (blue) $a_{M,SF}$, $a_{\phi,Q}$ and $b_{M,SF}$ by 1σ . Note that the distributions are normalised such that the integral over the redshift range $z \in [0, 3]$ is one. The columns correspond to the different survey types. The first column shows the results of SDSS-like surveys. The second and third columns display the results of DES- and HSC-like surveys, respectively. The rows correspond to the different parameters. Furthermore, we indicate the number of galaxies per square arcminute in the legends of each plot. We see that DES- and HSC-like surveys are more sensitive to $a_{M,SF}$, $a_{\phi,Q}$ and $b_{M,SF}$. Furthermore, $a_{M,SF}$ has the strongest impact.

similar characteristics. DES- and HSC-like surveys are more sensitive to $a_{\phi,Q}$ and increasing the parameter has a stronger effect than decreasing it. Especially, the plots indicate that a change of the parameters that increases the mean redshift has generally a stronger effect than a change that decreases the mean redshift. This attribute is independent of the direction of the parameter change and follows from the fact that fewer high-redshift than low-redshift galaxies are measured. The change that increases the mean redshift is also always accompanied by an increase in the number density. Hence, constraining the direction of change that is causing the increase in the mean redshift is more important than the direction that decreases the mean redshift.

Looking at the model of the characteristic magnitude (eq. 3), the above-mentioned observations agree with theoretical expectations. As a_M describes the redshift evolution of the characteristic magnitude, variations of a_M directly change the bright end of the luminosity function. Since galaxy observations are in general limited by the flux, the changes in the bright end influence the abundance of measured high redshift objects. Although b_M is also affecting the characteristic magnitude it does not affect the redshift evolution directly and is expected to have less impact on the redshift distribution than a_M .

The different survey types also have distinct sensitivity to the parameters of the two galaxy populations. Tables 8, 9 and 10 show that DES- and HSC-like surveys tend to be more sensitive to parameters of the star-forming population. On the other hand, SDSS-like surveys are more sensitive to the parameters of quenched galaxies. For DES- and HSC-like surveys, $a_{M,SF}$ has the strongest impact on the redshift

distribution. Conversely, the mean redshift of an SDSS-like survey is most sensitive to $a_{M,Q}$ and $b_{M,Q}$. The difference in the sensitivities follows from the variety in the depths of the surveys. An SDSS-like survey has a lower magnitude limit than the other surveys and measures mostly closer galaxies, which have lower redshift values. These galaxies had more time to get quenched and the ratio of star-forming to quenched galaxies is smaller than for DES- and HSC-like surveys. DES- and HSC-like surveys are more sensitive to parameters of the star-forming galaxies because these survey types also measure younger galaxies. However, the majority of galaxies measured by these surveys still have low redshifts. That explains why parameters of the quenched galaxies can have a strong impact on the redshift distribution of DES- and HSC-like surveys, for example, the 13.5 per cent change of the DES-like mean redshift or the 17.5 per cent change in the case of an HSC-like survey after decreasing $a_{M,Q}$.

To summarise the analysis of the sensitivity to the Schechter parameters, we found that $a_{M,SF}$ has the highest impact on the redshift distribution, although the sensitivity depends on the survey type. We conclude that $a_{M,SF}$ is the most important parameter to constrain. Within the given uncertainty of $a_{M,SF}$ the modelled mean redshift can change by up to 0.3. This can cause strong bias in the cosmological constraints when using weak lensing observations and the forward modelled redshift distribution. We present the most sensitive observables in the following section.

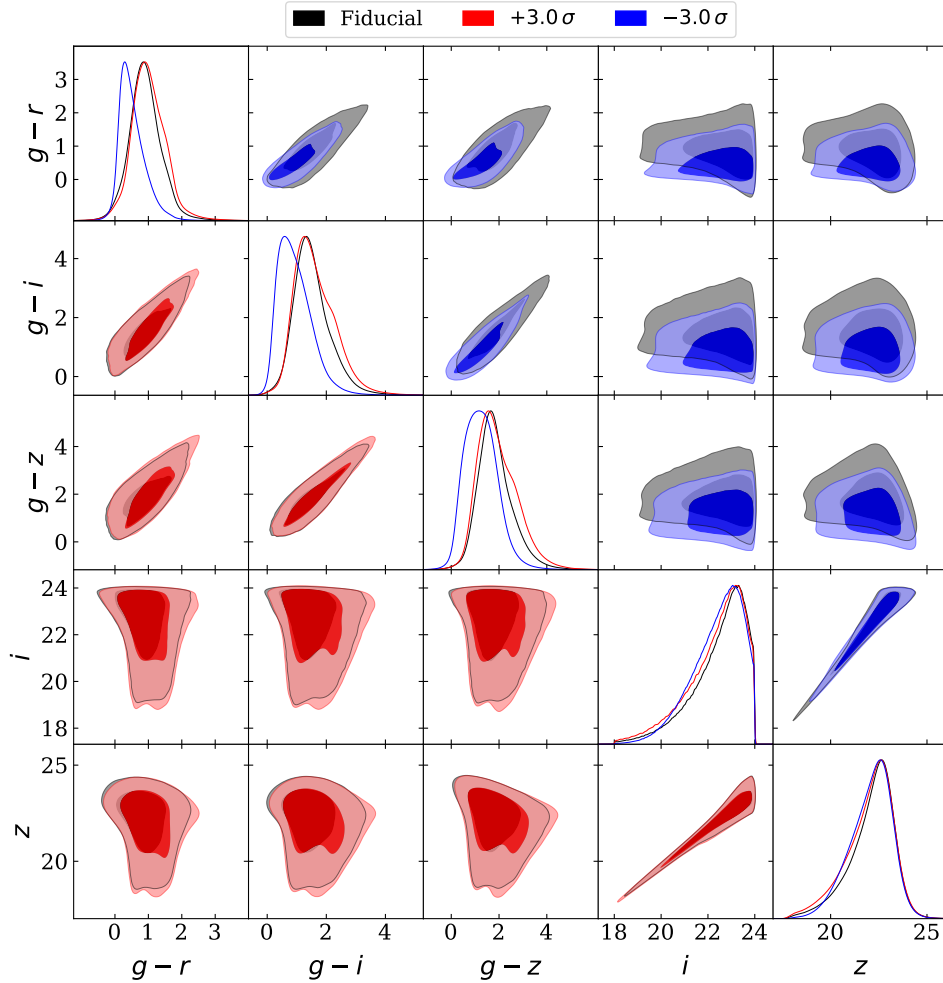


Figure 5. Corner plot of the $g-r$, $g-i$, $g-z$ colour and i - and z -band magnitude distributions for a **DES-like survey**. Black lines and contours correspond to the distributions in the fiducial catalogue. The red and blue colours represent the test catalogues after increasing and decreasing $a_{M,SF}$ by 3σ , respectively. The colour distributions are more affected by a change of $a_{M,SF}$. A combination of colour and magnitude is most suitable to constrain $a_{M,SF}$.

5.2 Colour and Magnitude Distributions

To investigate the effect of the parameter changes on the observables, we compared the magnitude and colour distributions of the fiducial and test catalogues. We focused on DES-like surveys because their depths are similar to those of future and upcoming surveys as previously mentioned. We investigated the effect on all observables (apparent magnitudes in the different bands and the corresponding colours) but concentrated on the five most sensitive observables to $a_{M,SF}$, which are the $g-r$, $g-i$, $g-z$ colour and i - and z -band magnitude distributions.

We focused on the results for $a_{M,SF}$ for two reasons. First, we showed that $a_{M,SF}$ causes the strongest effect and is most important to constrain. Second, we found that the to $a_{M,SF}$ most sensitive observables are generally sensitive to the other parameters as well. Especially, the colour distributions are very sensitive to changes in most of the parameters¹⁴.

We found that the colour distributions $g-r$, $g-i$, $g-z$ and the magnitude distributions in the i - and z -band are the five most sensitive observables to $a_{M,SF}$ and have the highest potential to help constraining its value in the future. As described earlier, we compared the colour and magnitude distributions of fiducial and test catalogues quantitatively using the Anderson-Darling test. In the case of the colour distributions $g-r$, $g-i$ and $g-z$, we obtained d-values of the order 10^4 after decreasing the parameter value. In the case of the magnitude distributions in the i - and z -bands, the d-values were of the order 10^3 . Hence, the colour distributions are more sensitive to a modification of $a_{M,SF}$ than the magnitude distributions. The d-value after decreasing the value of $a_{M,SF}$ by its error for the $g-r$ colour distributions was $\sim 21,300$. This value was the largest in our analysis.

Figure 5 shows a corner plot comparing these five observables. The plot contains the one-dimensional distributions and contours of all observables. The black lines and contours correspond to the fiducial catalogue. The colours blue and red represent the results of the test catalogue after

¹⁴ That is even true for the other survey types.

decreasing and increasing $a_{M,SF}$ by 3σ . Again, blue corresponds to a negative and red to a positive change.

The one-dimensional distributions in figure 5 verify the results indicated by the AD test that the colours are more sensitive to a change of $a_{M,SF}$ than the magnitudes. Once more, we observed that the negative change, which increases the mean redshift, has a stronger impact on the distributions than a positive change. The figure also shows that modifying the parameter affects the shape and the peak of the colour distributions. However, in the case of the magnitude distributions, the shapes are affected by the parameter change but the peaks stay the same. For different colour and magnitude choices in this comparison, the conclusion might be different because of the distinct sensitivity in the single bands.

The contours show that a combination of colour and magnitude is generally most sensitive to the parameters and might be the best choice to constrain them. The differences in the fiducial and test contours appear larger in colour-magnitude space. In addition, the results indicate that the magnitude-magnitude distributions are less sensitive to the parameters than the distributions in colour-colour space. However, the sensitivity of the colour-colour distributions is still smaller than in colour-magnitude space. Additionally, the choice of colour-magnitude combination does not influence the sensitivity to the parameter change because all test contours feature similar deviations from the fiducial contours. Note that our analysis showed that these colour-magnitude pairs are sensitive to the rest of the parameters as well and not only $a_{M,SF}$. The AD tests indicated high sensitivity of these observables to all parameters. In general, the contour plots for the other parameters are similar to figure 5 and only small deviations exist. Therefore, these pairs might also be able to help constraining the other parameters. Furthermore, our analysis has shown the same results if we chose colour-magnitude pairs that are not included in the figure (e.g $i - z$ or $r - i$). But, as mentioned, we included the colours and magnitudes with the highest sensitivity.

We also investigated the effect of modifying the Schechter parameters to HSC-like measurements. Figure 6 shows the same plot as figure 5 but for an HSC-like survey. Comparing the two plots illustrates that a deep HSC-like survey has higher sensitivity and therefore better constraining ability than a DES-like survey. The HSC-like contours of fiducial and test catalogues have a larger deviation than in the case of DES-like surveys. Furthermore, the one-dimensional colour and magnitude distributions are more responsive to the parameter modification. Although the d-values for a negative modification of the parameter are similar to the results of a DES-like survey, the d-values after adding the parameter error to its value are larger in the case of HSC-like measurements. The d-values of the colour distributions $g - r$, $g - i$ and $g - z$ are $\sim 6 \cdot 10^3$ in the case of HSC-like survey and, hence, about six times larger than in the case of DES-like surveys.

In summary, we suggest that a combination of colour-magnitude measurements is more sensitive to changes to the Schechter parameters and can be more useful to constrain them. Thereby, the exact selection of colour-magnitude pair has a minor role because the sensitivity is in general similar for all combinations. Additionally, HSC-like measurements can improve the constraining power compared to DES-like measurements.

6 CONCLUSIONS

Different cosmological probes are used to constrain the parameters of dark energy as well as dark matter and, therefore, to improve the cosmological model. One of these probes is weak gravitational lensing. Cosmic shear measurements rely on knowing the redshift distribution $n(z)$ of the galaxies under study. However, measuring $n(z)$ with sufficient precision is difficult. Spectroscopic redshifts are most accurate but current and upcoming experiments are too large to measure redshifts efficiently using spectroscopy. On the other hand, photometric redshifts do not have adequate precision.

Herbel et al. (2017) used a forward modelling approach to get a full posterior of $n(z)$ without having information about each individual redshift. Their model is based on redshift-dependent Schechter luminosity functions (see eq. 2). In this model, the characteristic magnitude is a linear function of redshift z and the amplitude has an exponential relation to z . The model includes two different galaxy types, star-forming (SF) galaxies and quenched (Q) galaxies. Therefore, the number of galaxies per comoving volume and absolute magnitude depends on the eight Schechter luminosity function parameters $a_{M,SF}$, $a_{M,Q}$, $a_{\phi,SF}$, $a_{\phi,Q}$, $b_{M,SF}$, $b_{M,Q}$, $b_{\phi,SF}$ and $b_{\phi,Q}$.

Throughout this paper, we investigated the sensitivity of the redshift distributions from DES-, HSC- and SDSS-like surveys to these parameters with the goal to identify which galaxy population features need to be well understood for future precision measurements. As the result of this and within the context of our forward model, we identified which Schechter parameters are most important to constrain such that the uncertainties of shear measurements are reduced. Additionally, we explored how the Schechter parameters affected the galaxy observables (magnitudes and colours). In this way, we identified the observables that are most sensitive to the Schechter parameters and that could help to constrain the parameters. We refer to section 4 for more details about our methodology.

We found that constraining $a_{M,SF}$ has the highest priority for simulating the redshift distribution of DES-like surveys. Since upcoming surveys like Euclid and LSST have similar properties as DES, having better constraints of $a_{M,SF}$ is especially important for future studies that are based on simulated redshift distributions. The uncertainty of $a_{M,SF}$ can affect the mean redshift by up to $\sim 45\%$, which corresponds to an absolute change of ~ 0.3 . The other parameters have less effect on the simulations but the results suggest that $a_{M,Q}$, $a_{\phi,SF}$, $a_{\phi,Q}$ and $b_{M,SF}$ require better constraints as well.

Furthermore, we found that the two-dimensional distributions in colour-magnitude space are generally more sensitive to the parameters than the distributions in colour-colour and magnitude-magnitude space. Therefore, the colour-magnitude distributions can help constraining the parameters, especially $a_{M,SF}$, the best. The results also show that the choice of the colour-magnitude combination has a minor role. In the case of a DES-like survey, we found that the $(g - r) - i$, $(g - r) - z$, $(g - i) - i$ and $(g - i) - z$ colour-magnitude combinations are the best options. However, HSC-like measurements might be a better choice to constrain the parameters because they have higher sensitivity to the Schechter parameters.

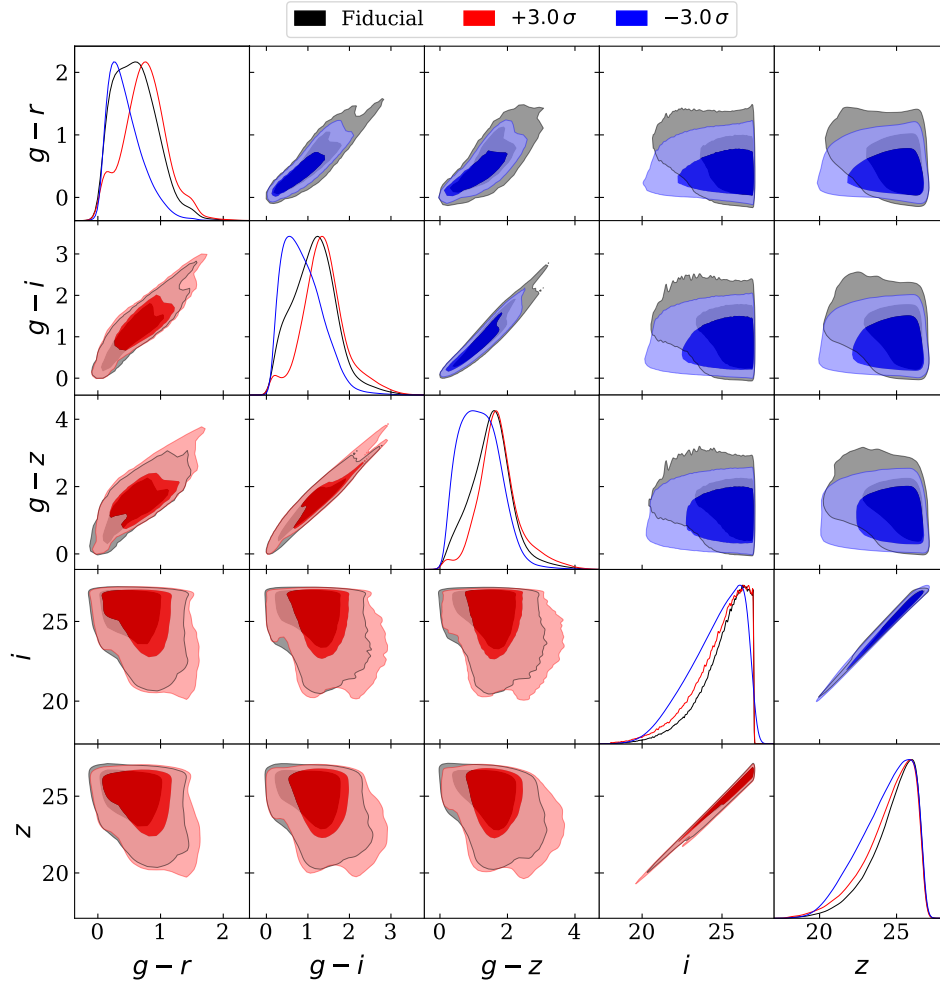


Figure 6. Corner plot of the $g-r$, $g-i$, $g-z$ colour and i - and z -band magnitude distributions for an **HSC-like survey**. Black lines and contours correspond to the distributions in the fiducial catalogue. The red and blue colours represent the test catalogues after increasing and decreasing $a_{M,SF}$ by 3σ , respectively. Comparing this plot with figure 5, we see that an HSC-like survey is strongly affected by the parameter change than a DES-like survey.

Finally, we will include the error model that is described in section 3.3.1 to the `skypy.utils` module of the `SkyPy` library (SkyPy Collaboration 2020; Amara et al. 2021). Additionally, we aim to improve the constraints of the parameters in future projects.

ACKNOWLEDGEMENTS

We would like to thank all our colleagues in the SkyPy Collaboration. We especially acknowledge N. Tessore and R. P. Rollins for many useful discussions in the early stages of this paper.

The preparation of this manuscript was made possible by a number of software packages: `NumPy` (Harris et al. 2020), `SciPy` (Virtanen et al. 2020), `Astropy` (Price-Whelan et al. 2018), `Matplotlib` (Hunter 2007), `IPython/Jupyter` (Perez & Granger 2007) and `GetDist` (Lewis 2019). This research partly developed and made use of `SkyPy`, a Python package for forward modelling astronomical surveys (SkyPy Collaboration 2020; Amara et al. 2021).

PS and AA acknowledge support from a Royal Society Wolfson Fellowship grant.

DATA AVAILABILITY

The data produced in this work will be available as the corresponding configuration files for the simulations in the `SkyPy` GitHub repository, <https://github.com/skypyproject/skypy> and <https://doi.org/10.5281/zenodo.4071945>.

The public data used in figures 1, 2 and 3 were obtained from Drlica-Wagner et al. (2018) at <https://des.ncsa.illinois.edu/releases/y1a1/gold>, Ahumada et al. (2020) at <http://skyserver.sdss.org/CasJobs/> and from Aihara et al. (2019) at <https://hsc-release.mtk.nao.ac.jp/datasearch/>, respectively.

REFERENCES

Abbott T. M. C., et al., 2018, *The Astrophysical Journal Supplement Series*, 239, 18

- Abdalla F. B., Amara A., Capak P., Cypriano E. S., Lahav O., Rhodes J., 2008, *Monthly Notices of the Royal Astronomical Society*, 387, 969
- Ahumada R., et al., 2020, *The Astrophysical Journal Supplement Series*, 249, 3
- Aihara H., et al., 2018, *Publications of the Astronomical Society of Japan*, 70, 1
- Aihara H., et al., 2019, *Publications of the Astronomical Society of Japan*, 71, 1
- Albrecht A., et al., 2006, e-prints arXiv:astro-ph/0609591
- Amara A., Réfrégier A., 2007, *Monthly Notices of the Royal Astronomical Society*, 381, 1018
- Amara A., et al., 2021, *Journal of Open Source Software*, 6, 3056
- Benitez N., 2000, *The Astrophysical Journal*, 536, 571
- Bergé J., Gamper L., Réfrégier A., Amara A., 2013, *Astronomy and Computing*, 1, 23
- Blanton M. R., Roweis S., 2007, *The Astronomical Journal*, 133, 734
- Blanton M. R., et al., 2003, *The Astronomical Journal*, 125, 2348
- Bolzonella M., Miralles J. M., Pelló R., 2000, *Astronomy and Astrophysics*, 363, 476
- Bordoloi R., Lilly S. J., Amara A., 2010, *Monthly Notices of the Royal Astronomical Society*, 406, 881
- Bordoloi R., et al., 2012, *Monthly Notices of the Royal Astronomical Society*, 421, 1671
- Capela F., Pshirkov M., Tinyakov P., 2013, *Physical Review D - Particles, Fields, Gravitation and Cosmology*, 87, 1
- Carrasco Kind M., Brunner R. J., 2013, *Monthly Notices of the Royal Astronomical Society*, 432, 1483
- Clifton T., Ferreira P. G., Padilla A., Skordis C., 2012, *Physics Reports*, 513, 1
- Drlaca-Wagner A., et al., 2018, *The Astrophysical Journal Supplement Series*, 235, 33
- Fagioli M., et al., 2018, *Journal of Cosmology and Astroparticle Physics*, 2018, 015
- Fagioli M., Tortorelli L., Herbel J., Zürcher D., Refregier A., Amara A., 2020, *Journal of Cosmology and Astroparticle Physics*, 2020, 050
- Feigelson E. D., Babu G. J., 2012, *Modern Statistical Methods for Astronomy*. Cambridge University Press, Cambridge, doi:10.1017/CBO9781139015653, <http://ebooks.cambridge.org/ref/id/CBO9781139015653>
- Flaugher B., et al., 2015, *Astronomical Journal*, 150
- Harris C. R., et al., 2020, *Nature*, 585, 357
- Herbel J., Kacprzak T., Amara A., Refregier A., Bruderer C., Nicola A., 2017, *Journal of Cosmology and Astroparticle Physics*, 2017
- Hogg D. W., Baldry I. K., Blanton M. R., Eisenstein D. J., 2002, arXiv e-prints:astro-ph/0210394
- Honscheid K., DePoy D. L., 2008, e-prints arXiv:0810.3600
- Hunter J. D., 2007, *Computing in Science & Engineering*, 9, 90
- Kawanomoto S., et al., 2018, *Publications of the Astronomical Society of Japan*, 70, 1
- Kotz S., Balakrishnan N., Johnson N., 2019, in , *Continuous Multivariate Distributions. Volume 1: Models and Applications*, 2nd edn, Wiley, <https://books.google.sh/books?id=VIgbEAAAQBAJ>
- Lewis A., 2019, e-prints arXiv:1910.13970
- López-Sanjuan C., et al., 2017, *Astronomy and Astrophysics*, 599
- Loveday J., et al., 2012, *Monthly Notices of the Royal Astronomical Society*, 420, 1239
- Miyazaki S., et al., 2012, *Ground-based and Airborne Instrumentation for Astronomy IV*, 8446, 84460Z
- Nicola A., Refregier A., Amara A., 2017, *Physical Review D*, 95
- Perez F., Granger B. E., 2007, *Computing in Science & Engineering*, 9, 21
- Price-Whelan A. M., et al., 2018, *The Astronomical Journal*, 156, 123
- Rykoff E. S., Rozo E., Keisler R., 2015, eprint arXiv:1509.00870
- Sadeh I., Abdalla F. B., Lahav O., 2016, *Publications of the Astronomical Society of the Pacific*, 128, 1
- Salvato M., Ilbert O., Hoyle B., 2019, *Nature Astronomy*, 3, 212
- Schechter P., 1976, *The Astrophysical Journal*, 203, 297
- Scholz F. W., Stephens M. A., 1987, *Journal of the American Statistical Association*, 82, 918
- SkyPy Collaboration 2020, SkyPy, doi:10.5281/zenodo.4071945
- Spergel D. N., 2015, *Science*, 347, 1100
- Stoughton C., et al., 2002, *The Astronomical Journal*, 123, 485
- Tessore N., Harrison I., 2020, *The Open Journal of Astrophysics*, 3
- The Dark Energy Survey Collaboration 2005, e-prints arXiv:astro-ph/0510346
- Tortorelli L., et al., 2018, *Journal of Cosmology and Astroparticle Physics*, 2018
- Tortorelli L., Fagioli M., Herbel J., Amara A., Kacprzak T., Refregier A., 2020, *Journal of Cosmology and Astroparticle Physics*, 2020
- Tortorelli L., et al., 2021, e-prints arXiv:2106.02651
- Virtanen P., et al., 2020, *Nature Methods*, 17, 261
- York D. G., et al., 2000, *The Astronomical Journal*, 120, 1579

APPENDIX A: PLOTS REDSHIFT DISTRIBUTIONS

In this part of the paper, we visually compare the sensitivity of the redshift distributions to all Schechter parameters for the three survey types. The individual plots show the fiducial redshift distributions in black. The redshift distributions of the test catalogues after increasing and decreasing the parameters by their given errors are shown in red and blue, respectively. The legends of each plot contain the galaxy number density for each catalogue. Figure A1 shows the distributions of a DES-like survey. Figures A2 and A3 correspond to an HSC- and an SDSS-like survey, respectively. The plots are all in agreement with the results in section 5.1.

This paper has been typeset from a $\text{\TeX}/\text{\LaTeX}$ file prepared by the author.

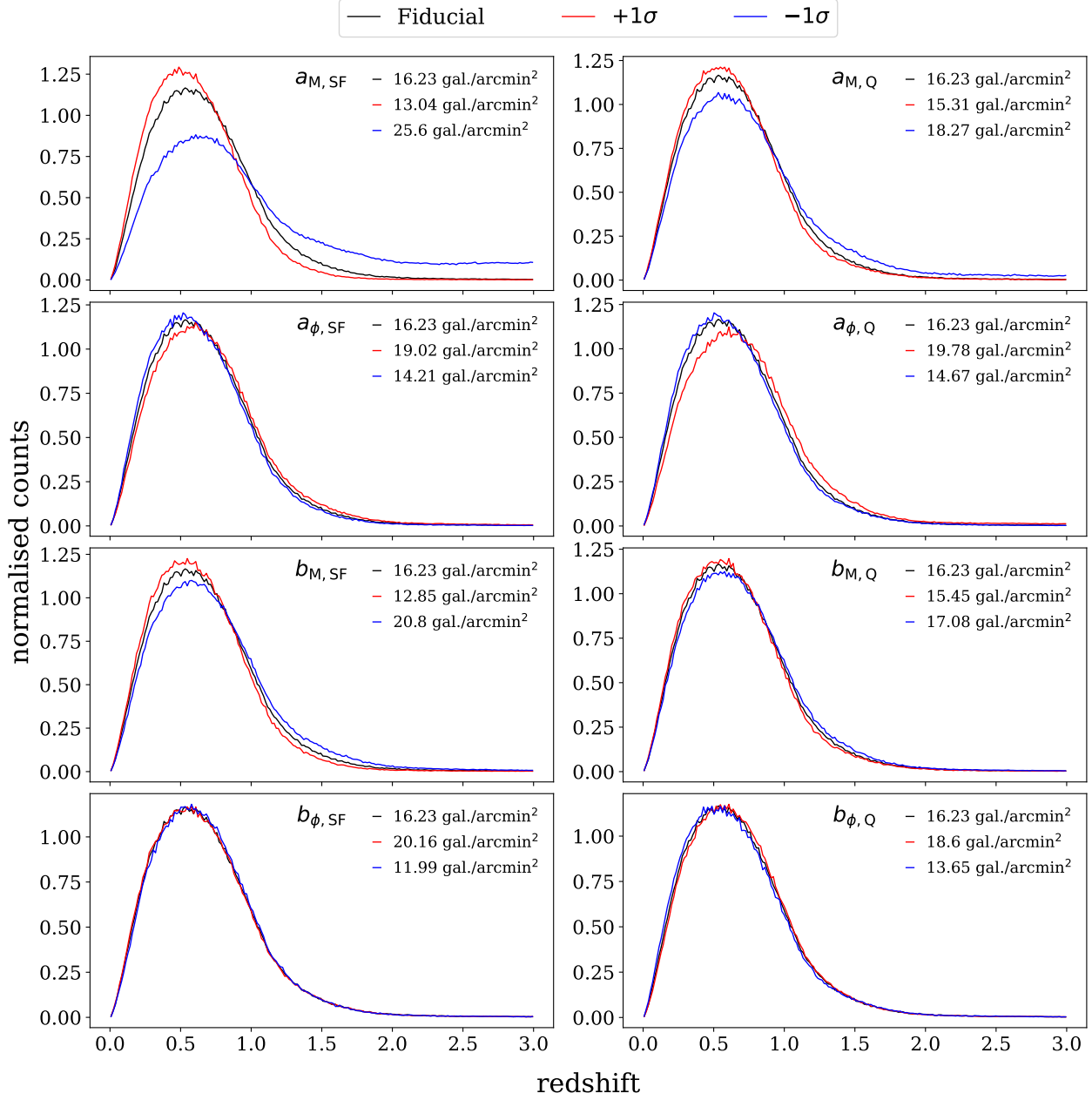


Figure A1. Comparison of the normalised simulated fiducial (black) and test redshift distributions of a **DES-like survey**. The red and blue lines correspond to increasing and decreasing the Schechter parameter by 1σ , respectively. The number of galaxies per square arcminute is indicated in the legend of each plot. The plots are in agreement with the results in section 5.1.

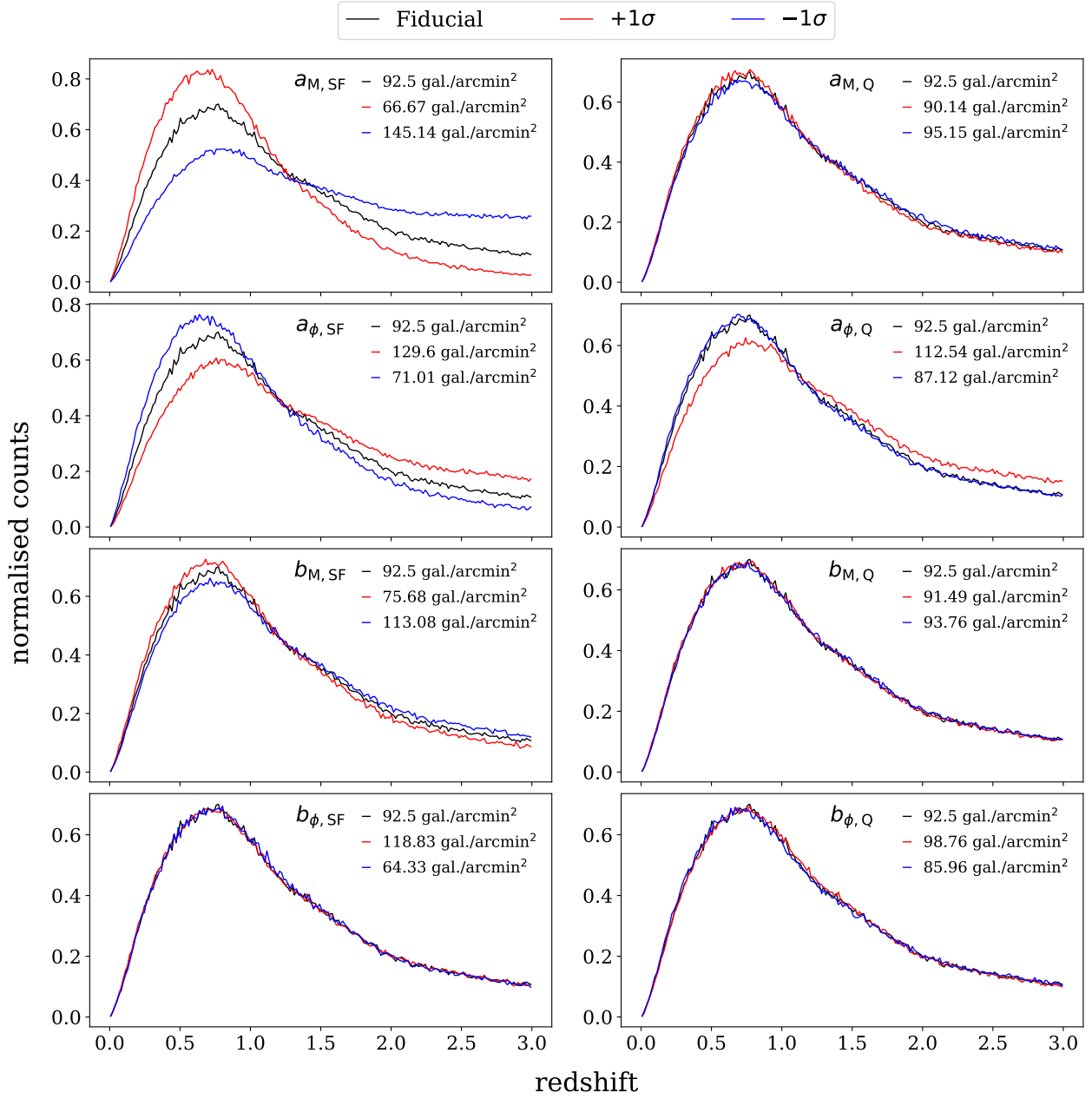


Figure A2. Same as A1 but for an HSC-like survey.

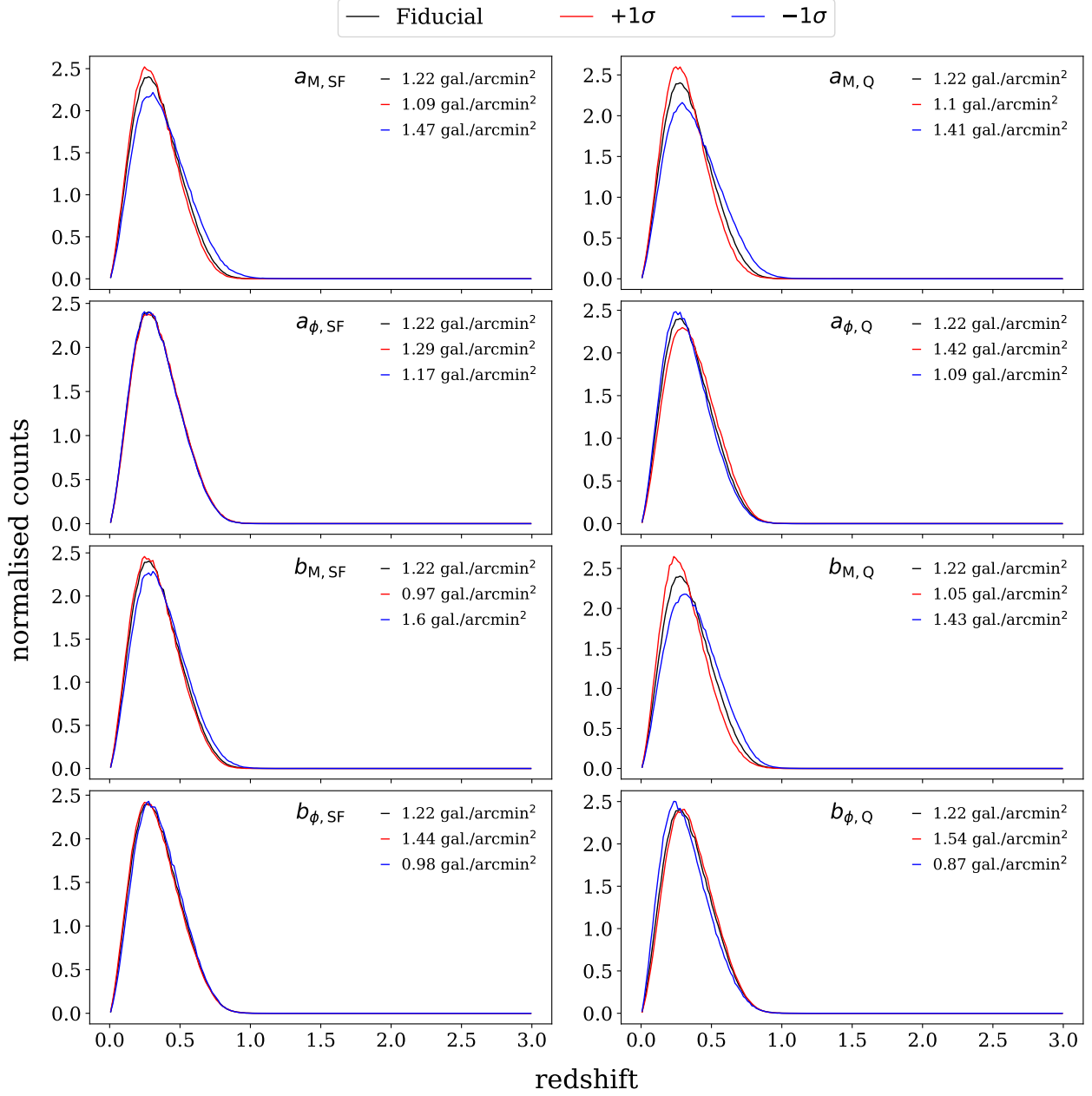


Figure A3. Same as A1 but for an SDSS-like survey.